Kinetics of anticrossing between slip traces and vicinal steps on crystal surfaces

C. Coupeau, D.M. Kazantsev, M. Drouet, V.L. Alperovich

Version of Record: https://www.sciencedirect.com/science/article/pii/S1359645419303775
Manuscript_103e44555e6449aeb9052335f2e7454c

Kinetics of anticrossing between slip traces and vicinal steps on crystal surfaces

C. Coupeau[1,*], D.M. Kazantsev[2,3], M. Drouet[1], V.L. Alperovich[2,3]

[1]*Pprime Institute, Department of Physics and Mechanics of Materials, University of Poitiers/CNRS/ENSMA, France*

[2]*Rzhanov Institute of Semiconductor Physics, 630090 Novosibirsk, Russia*

[3]*Novosibirsk State University, 630090 Novosibirsk, Russia*

**Corresponding author: christophe.coupeau@univ-poitiers.fr*

Abstract. The interaction between vicinal atomic steps and slip traces – straight monatomic steps produced on a crystal surface by the emergence of dislocations – is experimentally investigated and compared to Monte-Carlo simulations. Near the point of apparent crossing between a vicinal step and a slip trace, a checkered three-level surface relief configuration is formed, with two new combinatory steps that borders the opposite highest and lowest terraces. This configuration is unstable with respect to an anticrossing effect which consists in the formation of a nanometer scale bridge that separates the regions with the highest and lowest levels and connects the opposite regions of equal level. It is shown that such an anticrossing effect is a general phenomenon observed on various crystal surfaces, from metals to semiconductors. The anticrossing kinetics was experimentally investigated on the Au(111) surface by scanning tunneling microscopy under ultra-high vacuum. It is observed that the bridge width increases with time according to the power law with exponent $\beta = 0.45 \pm 0.01$, *i.e.* significantly smaller than for the single-particle diffusion ($\beta = 0.5$). Monte-Carlo simulations were performed in order to clarify the involved atomic diffusion mechanisms. In particular, the competition between two microscopic mechanisms of the bridge formation is discussed, *i.e.*, the adatom diffusion along the combinatory steps *versus* across the bridge from the uppermost to the lowest terrace.

Keywords: Vicinal surface; Slip traces; Anticrossing; Surface atomic diffusion; Au(111) surface

1. Introduction

Atomic steps at crystal surfaces are the basic morphological elements that determine the mechanisms of crystal growth, sublimation, wet or gas etching and other technologically important processes [1]. Well-prepared vicinal crystal surfaces, which are misoriented from a singular crystallographic face, exhibit regular sets of atomically smooth terraces separated by 'vicinal' steps of monatomic height, with the width of terraces determined by the misorientation angle [2,3]. Another type of atomic steps is caused by the dislocations emerging at the free surface [4,5], which may be inherited from a substrate under epitaxial growth or introduced due to the relaxation of external mechanical stresses. These latter steps are called slip traces as long as their directions are characteristic of the gliding of dislocations in their crystallographic planes [6-12]. Various phenomena on crystal surfaces involving each type of these steps were extensively studied and well understood. The formation of step-terraced morphology, step bunching and anti-bunching phenomena induced by the interaction of vicinal steps, electric current or adsorbates were studied on various semiconductor and metal surfaces [2,3,13-15]. On the other hand, scanning probe microscopy of dislocation-induced slip trace structures at free surfaces proved to be an effective tool for studying various phenomena associated with dislocation behaviour in crystals, such as partial splitting of screw dislocations [5,7], as well as plastic relaxation processes at nanoscale level under nanoindentation [8-11]. Misfit dislocations and dislocation-induced atomic steps are responsible for the formation of the well-known 'cross-hatched' relief patterns of mesoscopic heights on the surfaces of epitaxial films grown on the mismatched substrates, which can be seen by an optical microscope or even with a naked eye [16]. However, vicinal and slip steps of monatomic height were not clearly observed simultaneously until a recent study on a smooth gold surface [17]. This latter study was performed by means of an original experimental apparatus, 'Nanoplast', allowing to examine surface morphology evolution by atomic force microscopy or scanning tunnelling microscopy under ultra-high vacuum environment during *in situ* straining experiments performed over a large range of temperatures (90 to 600 K) [18]. The 'Nanoplast' apparatus provides a decisive step forward in studying elementary plastic relaxation processes due to the opportunity to observe directly the *in situ* evolution of slip traces produced, under increasing controlled strain, by newly born dislocations. In

particular, the crystallographic path followed by only one screw dislocation in Nb crystals has been recently studied [12]. This apparatus also made it possible to observe for the first time, under external stress, the regular arrays of both vicinal steps and slip traces on Au(111) surface [17].

Simultaneous observations of vicinal steps and slip traces enable us to clarify an old question about the crossing of atomic steps on a crystal surface. According to the theoretical considerations by Nozieres [19], atomic steps cannot cross. Indeed, if one supposes that two atomic steps cross, a checkered three-level relief configuration is created with the highest and the lowest regions being opposite to each other and different in height by two monolayers, while the other two opposite regions are of equal intermediate height. To keep a valid definition of a monatomic step that separates two surface regions which differ in height by one monolayer, two initial intersecting steps should be redefined by exchanging their ends into two new 'combinatory' steps with abrupt turns at the point of contact. This configuration with the touching angles of combinatory steps is unstable because the atomic diffusion along the steps or from the highest region to the opposite lowest region leads to an effective repulsion of the new steps and formation of an 'anticrossing bridge' that connects the two opposite regions with the intermediate height level.

For vicinal crystal surfaces, Nozieres reasoning seems purely theoretical because vicinal steps never cross each other. They can only touch and, thus, form steps of multiple heights or step bunches. In contrast, slip traces result from the dislocation gliding in specific crystallographic planes [20]. Slip traces are, thus, aligned along certain crystallographic directions and can cross vicinal steps. An apparent intersection of a monatomic vicinal step and a slip trace makes it possible to confirm the Nozieres theoretical idea and to experimentally explore the anticrossing configuration. In particular, Coupeau *et al.* observed, for the first time, the formation of a checkered relief structure and an anticrossing bridge resulting from the crossing of a single slip trace and a vicinal step on Au(111) surfaces [17]. A similar interplay between vicinal steps and slip traces was observed on the smooth vicinal surfaces of GaAs/AlGaAs structures bonded to glass, due to the partial plastic relaxation of thermo-mechanical stresses under annealing in quasi-equilibrium conditions [21].

Although the coexistence of vicinal and slip steps was experimentally demonstrated and the formation of anticrossing configuration is now qualitatively explained on Au(111) and on GaAs(001), a quantitative description of this phenomenon is still lacking, and a number of basic questions remain open. The main questions are related to the bridge width kinetics and to the involved microscopic mechanisms leading to the formation of anticrossing relief configuration. In particular, the anticrossing configuration can be formed by 'smoothing' abrupt turns of the combinatory steps due to the atomic diffusion along the steps (step diffusion mechanism, SDM). Another, 'recombination' mechanism (RM) consists in the atomic diffusion between the combinatory steps, across the bridge, from the uppermost to the lowest terrace. This diffusion leads to effective step repulsion and to the broadening of the bridge at the intermediate level. The question is, which of these two mechanisms, SDM or RM, plays a dominant role in the formation of anticrossing configuration? This question can be answered by an experimental study of the bridge width kinetics and by comparing the results to a theory that accounts for both mechanisms, but experimental and theoretical data on the kinetics have not been available in literature so far.

As the bridge formation is due to surface diffusion, one may assume that the bridge width w would be proportional to the square root of time $w \sim t^{1/2}$ with an 'effective' diffusion coefficient. A more careful analysis should take into account that, in the process of bridge formation, atoms should diffuse to distances which increase with time and step curvature radii. Therefore, similar to the relaxation of macroscopic relief features [1,22,23], a bridge width kinetics with a power smaller than ½ might be expected.

This paper is aimed at answering these questions by means of combined experimental investigations of the anticrossing configuration kinetics on strained Au(111) single crystals by UHV-STM and Monte-Carlo simulations. The results enabled us to clarify the microscopic mechanisms of the step interaction and to obtain the parameters that determine the kinetics of anticrossing bridge width formation on the Au(111) surface, such as diffusion activation and lateral bond energies.

2. Methods

2.1 Experimental

The Au single crystals of nominal section 2x2 mm^2 and 6 mm length were prepared by Surface Preparation Lab [24]. The Au(111) surfaces were first oriented with an accuracy better than 0.1°. After a chemical/mechanical polishing up to a Rms roughness lower than 30 nm, the Au(111) surface was prepared under the UHV environment ($<10^{-10}$ mbar) by repeated cycles of Ar ion bombardments (0.9 kV) and annealing at 850 K for 10 min. As expected, after a few cycles, the surface exhibits atomically flat {111} terraces separated by the vicinal steps of height $h_V = 240 \pm 10$ pm, close to the theoretical value of 235 pm. The samples were then mechanically strained in UHV conditions at low temperature $T = 180$ K and heated up to room temperature (RT) using a home-made experimental device allowing us to characterize, by UHV-STM, the *in situ* evolution of surfaces under increasing controlled strain (see [18] for details). The uniaxial compression was applied along the $[\bar{1}10]$ direction. From crystallographic considerations, the {111}<110> slip systems are expected to be activated in gold single crystals [7], with slip traces lying along the $[01\bar{1}]$ and $[\bar{1}01]$ directions at the Au(111) surface, *i.e.* at ± 60° from the compression axis. It is recalled that the height of a single trace corresponds to the Burgers vector $\vec{b}$ component perpendicular to the surface. Theoretically, $h_T = \vec{b}.\vec{n} = \frac{a}{\sqrt{3}} = 0.235$ nm, where $\vec{n}$ is the normal to the free surface and $a = 0.408$ nm is the lattice parameter for gold. It is noticed here that a single trace, *i.e.* a trace related to the emergence of only one perfect dislocation, has the same height as a vicinal step.

2.2 Monte Carlo simulations

The Monte Carlo simulations of the surface smoothing and step-terrace morphology formation were performed on the Kossel crystal in the standard solid-on-solid (SOS) model [25]. The complex processes of mass transfer on a real reconstructed

Au(111) surface are replaced by a random walk and attachment/detachment of Au atoms. The atoms are allowed to hop to adjacent free sites on a terrace, to incorporate into a step or to leave a step. The probability P (per second) of each event is determined through the activation energy E of the respective event, $P = \nu_0 e^{-E/k\mathrm{T}}$, where $\nu_0 \sim 10^{13}$ Hz is the Debye frequency, k is the Boltzmann constant, and T is the temperature. The energy E for the atomic surface diffusion is given by:

$$E = E_d + E_b(N_i - N_f)\Theta(N_i - N_f), \quad (1)$$

where E_d is the adatom diffusion activation energy, E_b is the binding energy, N_i and N_f are the lateral bond numbers of the atom before and after the hop, respectively and $\Theta(N)$ is the step-like function equal to one for $N_\mathrm{i} > N_\mathrm{f}$ or zero otherwise.

The desorption was neglected in agreement with the relatively low temperature of our experiments (close to or lower than room temperature). The computer program used earlier [26] was further developed in order to speed up the calculations. In particular, a reverse calculation algorithm was introduced. This algorithm consists in (i) computing the probabilities of all possible events, (ii) randomly selecting the events taking into account their probabilities, and (iii) updating the affected event probabilities and repeating step (ii). The reverse algorithm allowed us to increase the calculation speed by one or two orders of magnitude and, thus, to simulate processes on areas equal to experimental ones within a reasonable time.

In the simulations, the lattice constant of the Kossel crystal a_0 was set equal to the monatomic step height at the Au(111) surface, $h_\mathrm{V} = 0.235$ nm. The size of the simulated box L was in the range of (240-480) a_0, *i.e.* (56-112) nm. To keep the number of atoms constant, two different boundary conditions were used. For the periodic boundary conditions, each adatom that diffuses outside a simulated box boundary appears at the opposite boundary. For the infinite barrier boundary conditions, the adatom diffusion across the boundaries was forbidden. We proved that the results do not significantly depend on both the box size and the boundary conditions for $L \geq 240\ a_0$. In particular, under the increase of the box size L from 240 a_0 to 480 a_0, the bridge width increases only by less than 2% for both types of boundary conditions.

3. Results and discussion

The basic features of the interaction between vicinal steps and slip traces are illustrated in Fig. 1 by the UHV-STM images of the Au(111) sample, which were measured after plastic deformation at low temperature $T = 180$ K (Fig. 1a) and after a subsequent one-hour anneal at room temperature (Fig. 1b). Prior to deformation, the surface exhibited atomically flat terraces separated by curved vicinal steps of monoatomic height 0.235 nm labelled from V_1 to V_7. The plastic strain of $\varepsilon_p = 0.29\%$ leads to the appearance of straight vertical slip traces labelled T_1 and T_2, which lie in the $[01\bar{1}]$ direction and cross the vicinal steps. In this case, the crystal shearing by a dislocation corresponds to the uplift of the material on the right side of the slip trace by an amount of 0.235 nm. Thus, as expected, here the slip traces, which are, essentially, the dislocation-induced monatomic steps, have the same height as vicinal steps. This height corresponds to the Au crystal period in the direction normal to the (111) surface.

At first glance, the sets of curved vicinal steps and straight slip traces in Fig.1a look like seemingly independent, with each vicinal step and slip trace apparently kept intact. However, a more careful analysis of the resulting relief proves that the introduction of slip traces leads to a radical reorganization of the atomic step system, with the formation of new combinatory steps from the former vicinal steps and slip traces. Indeed, as it is seen in Fig. 1a, a 'checkered' relief is formed near each crossing point. This specific relief is characterized by four terraces around the crossing point, at three sequential atomic levels labelled 0, 1 and 2, as highlighted in the white frame near the intersection between V_6 and T_1. The lowest and the highest opposite terraces differ in height by two monolayers, while the other two opposite terraces are at the same intermediate level. Despite intuitive considerations of step lines 'continuity', due to the crossing, neither the initial vicinal steps, nor the slip traces can be anymore considered as atomic steps in the conventional definition, which implies that a monatomic step separates two adjacent terraces with the difference in height equal to one monolayer. Instead, new 'combinatory' atomic steps, with sharp angles at crossing points, are

formed, by exchanging the ends of the former steps. The segments of two new combinatory steps C_0 and C_2 near the intersection between V_6 and T_1 are highlighted by dotted and dashed white lines, respectively. The combinatory step C_0 borders the lowest terrace of the checkered relief and consists of the left part of V_6 and the upper part of T_1, while C_2 borders the highest terrace and consists of the right part of V_6 and the lower part of T_1.

At low temperatures $T \leq 180$ K, the checkered surface relief with the touching angles of the new combinatory steps (Fig. 1a) did not significantly evolve for more than one hour. In contrast, at higher (room) temperature, such a structure was shown to be unstable and evolved to the structure that is shown in Fig. 1(b), with curved combinatory steps and a few nanometers wide 'bridge' that separates the lowest and highest terraces and links the opposite terraces with the same intermediate atomic level [17]. This evolution, which is likely caused by the atomic diffusion along the steps and from the highest to the lowest terrace, is called the anticrossing phenomenon in the following. It is clearly seen in Fig. 1b that the anticrossing occurs everywhere on the sample surface. In Fig. 1(b) the combinatory steps C_0 and C_2 are highlighted throughout the whole image in order to visualize the formation of staircase of twisted combinatory steps, with each step consisting of interleaving curved segments of former vicinal steps and relatively straight vertical segments of former slip traces.

We showed experimentally that the anticrossing behavior is a universal phenomenon occurring in a large variety of materials, from simple and compound metals (see Fig. 2a, b and c for Au and Ni_3Al) to semiconductors (see Fig. 2d for GaAs). A similar step pattern was experimentally evidenced on rock salt as well [27]. Figs. 2a and 2b show a zoomed STM image of an anticrossing bridge formed on the Au(111) surface and a characteristic profile across the bridge along the dashed line. The image and the profile highlight the three sequential atomic levels of the resulting terraces. The image of the anticrossing configuration on the $Ni_3Al(111)$ surface shown in Fig. 2c was obtained in the same UHV-STM set-up, in the course of an experiment similar to that performed on Au(111). In Fig. 2c, the heights of both the vertical slip trace T and the inclined vicinal step V are equal to 0.208 nm, *i.e.* to the period of Ni_3Al in the [111] direction.

Checkered relief configurations around multiple intersections between monatomic curved vicinal steps (labelled V_1-V_3) and straight slip traces (T_1-T_3) are clearly seen in the topographical image of the GaAs(001) surface (Fig. 2d). The image was taken by atomic force microscopy (AFM), after the one-hour anneal of a glass-bonded GaAs/AlGaAs heterostructure at relatively high temperature $T = 820$ K [21]. The AFM measurements were done on the equipment of CKP "Nanostructures" (Novosibirsk). The height of all steps in Fig. 2d is equal to the period of GaAs in the direction normal to the (001) plane (≈ 0.28 nm), *i.e.* corresponds to the Ga-As bilayer thickness in this direction [21]. Unlike the uniaxial deformation applied to Au(111) and Ni_3Al(111) samples [17,18], the partial relaxation of thermo-mechanical biaxial stress in the GaAs/AlGaAs heterostructure led to the formation of a rectangular grid of slip traces oriented in the [110] and $[1\bar{1}0]$ directions. As a result, along with the checkered relief configurations due to the intersections of the slip traces with vicinal steps, checkered configurations are formed due to the intersections of mutually orthogonal dislocation-induced steps with each other; two of such configurations corresponding to the intersections between T_3 with T_1 and T_2 are clearly seen in the right part of Fig. 2d. It is also seen in Fig 2d that, in contrast to the slip traces on Au(111) (see Fig. 1), the signs of two parallel slip traces T_1 and T_2 are opposite: when going from top to bottom, trace T_1 corresponds to the uplift, while T_2 corresponds to the lowering of the next terrace. The adjacent dislocation steps may have the opposite signs because, in GaAs, the dislocation loops, which are introduced in the (111) and $(\bar{1}\bar{1}1)$ planes, have opposite signs of the Burger's vector normal component and, thus, produce parallel slip steps of the opposite signs on the GaAs(001) surface. Therefore, on GaAs(001), the dislocation steps form a set of orthogonal stripes with non-monotonically interleaving lower and higher lying terraces [21]. Such morphology is in contrast to a fragment of a vicinal surface with a certain sign of the misorientation angle, on which the vicinal step steps have the same sign and, thus, form a monotonically descending (or ascending) staircase. It should be noted that the lateral AFM resolution was by an order of magnitude lower, compared to the UHV-STM resolution of Au(111) and Ni_3Al(111) images shown in Figs. 2a and 2c, respectively. Consequently, anticrossing bridges are not clearly seen in Fig. 2d. At higher annealing temperatures, the bridges on the GaAs(001) could be

observed [21], but still not so clearly compared to the UHV-STM images of Au and Ni_3Al.

It should be noted that, although the anticrossing phenomenon is proved to be a universal phenomenon, on semiconductor surfaces it occurs at much higher temperatures than on metal surfaces; in particular, at T ~ 800-900 K on GaAs [21] versus T ~ 300 K on Au [17]. A likely explanation consists in relatively small values of metallic bonds and diffusion activation energies that facilitate surface diffusion, in contrast to semiconductor surfaces with higher bond and diffusion activation energies, covalent dangling bonds and unscreened surface potential undulations that hinder diffusion at low temperatures.

The kinetic evolution of a characteristic checkered structure measured by UHV-STM on the Au(111) surface at $T = 297$ K is shown in Fig. 3. The slip trace (*resp*. the vicinal step) is labelled *T* (*resp*. *V*). Despite quite low lateral resolution in Fig. 3a induced by the high scanning rate needed to catch the anticrossing kinetics, the sequence of the images, which were taken at various durations after the dislocation emergence, clearly evidences the growth of the bridge. A well-known Au(111) reconstruction, called herringbone or chevron-like pattern [28-31], is seen in Fig. 3c (see the area on the right terrace on which the contrast has been enhanced). It is also seen in Fig. 3c that the segments of the combinatory steps, which originated from slip trace T, remained atomically straight. In contrast, the upper segment of the right-side combinatory step, which originated from the vicinal step, is not straight and contains clear ledges, presumably corresponding to kink bunches.

The bridge width w was extracted from the UHV-STM images by approximating the curved steps by arcs with a constant curvature radius. The time-dependence of w is shown in Fig. 4 in the double log scale for two experiments at $T = 297$ K (circles) and $T = 278$ K (triangles). The experimental data at 297 K (*resp*. at 278 K) correspond to crossing angle $2\alpha = 60°$ (*resp*. $2\alpha = 48°$). Here, 2α is defined as the angle between the slip trace T and the vicinal step V on the middle terrace of level 1 (see Fig. 3c). The error was estimated by measuring the widths of various bridges observed in the STM images. It is seen that, in both experiments, the bridge width logarithm $\ln(w)$ evolves approximately linearly with $\ln(t)$, and this evidences a power dependence $w(t) \sim t^{\beta}$.

We performed Monte Carlo simulations (MCS) of anticrossing bridge formations in order to elucidate the involved mechanisms. The simulated kinetic evolution of the checkered structure is shown in Fig. 5. The initial checkered configuration resulting from the crossing between a slip trace and a vicinal step at $2a = 60°$ is shown in Fig. 5a. Note that the slip trace is perfectly straight due to its singular orientation, while the inclined vicinal step, which is misoriented from the singular direction, contains atomic size kinks. The simulated evolution of the checkered relief after annealing at room temperature $T = 297$ K is shown in Figs. 5b-d for the increasing annealing time. It is evidenced that the initial checkered configuration with the touching angles of new combinatory steps is unstable, and the anticrossing configuration develops as a result of the annealing. As expected, the bridge width monotonically increases with the annealing time. It can be seen that, at least at the initial stage of the bridge formation, the slip trace remains nearly straight (Fig. 5b) or evolves into a regular array of straight (vertical) segments separated by monatomic kinks (Fig. 5c). In contrast, the vicinal step segments acquire a noticeable roughness. Such a roughness apparently stems from a kink ripening on the vicinal segments, not observed on the slip trace segments due to their initially straight character.

The comparison of experimental UHV-STM images shown in Fig. 3 with the simulated images in Fig. 5 proves that the MCS qualitatively describes the kinetics of anticrossing configuration. In order to perform a quantitative comparison, elucidate the relevant microscopic mechanisms and determine the model parameters, we compared the experimental and simulated kinetics of the bridge width $w(t)$. To extract the bridge width from the simulated images, similar to the experimental procedure, the combinatory steps were approximated by arcs in the vicinity of anticrossing, as shown with the dashed lines in Fig. 5d. The shortest distance between the arcs, that was averaged over 64 anticrossing simulations with the same parameters, was taken as bridge width w. The experimental kinetics measured at 297 K and 278 K was best-fitted by MCS with the same set of model parameters. The simulated kinetics $w(t)$ are shown in Fig. 4 with the solid lines. It can be seen that the experimental and simulation kinetics agree reasonably well. The departure of one point of the 297 K kinetics outside the error bar can be hardly treated as a significant deviation of the experiment from the simulation, although, keeping in mind the simplicity of the model, the deviations might

be expected. In the double log scale, the kinetics are approximated by straight lines, which correspond to a power dependence of the bridge width on time as $w(t) \sim t^{\beta}$. In the simulations, the diffusion activation energy was first fixed and taken from literature $E_d = 0.4$ eV [32,33], while the fitting parameter (lateral bond energy) turned out to be $E_b = 0.204 \pm 0.001$ eV. For the kinetics measured at $T = 278$ K, additional simulations with E_b deviated from the best fit value by only ± 0.005 eV proved that the resulting simulated kinetics are shifted by about $\pm 20\%$ from the experimental kinetics. This shift demonstrates the high sensitivity of the fitting procedure to the model parameters.

It should be noted, however, that it is not possible to determine definitely both E_d and E_b by fitting the experimental kinetics with MCS. More specifically, the deviation of the simulation curve from the experiment, which is caused by changing the lateral bond energy E_b, can be compensated by an appropriate change in the diffusion activation energy E_d. The description of the bridge width kinetics is, therefore, a one-parameter rather than a two-parameter problem. In other words, the experimental kinetics can be successfully approximated by simulations with various, but strongly correlated pairs of E_d and E_b. The plot of $E_b(E_d)$ corresponding to such pairs calculated for $2\alpha = 60°$ is shown in Fig. 6 by circles. It is seen that the dependence E_b *vs*. E_d is well described with a straight line. Along this line, the variations of the χ^2 criterion were below 2%. In an attempt to determine both E_d and E_b separately, we tried to use experiments with different intersection angles 2α. However, it turned out that the correlation of E_b *vs*. E_d does not depend on the intersecting angle 2α, since no significant change is observed in the nearly extreme cases of ultimately small $2\alpha = 15°$ (dotted line) and large $2\alpha = 165°$ (dashed line) angles.

It is seen in Fig. 4 that the experimental and simulated kinetics are well approximated by a power dependence $w(t) \sim t^{\beta}$. The magnitude of the exponent β as a function of E_d is shown in Fig. 6 by triangles. It can be seen that β does not depend on E_d and is equal to $\beta = 0.45 \pm 0.01$. This value is distinctly lower than $\beta = 0.5$, characteristic of a single particle diffusion [1]. This lower value of β may be related to the increase with time of the distance at which atoms should diffuse in order to form an anticrossing bridge. Similarly, it is known that the amplitude of macroscopic relief waves evolves towards flat surfaces by massive surface diffusion as $t^{1/4}$ [1,22]. Thus, in

our case of surface diffusion that forms a two-dimensional anticrossing relief configuration, exponent β turns out to have an intermediate value between those characteristic of the single particle diffusion and the relaxation of 3D macroscopic relief features.

The anticrossing bridge can be formed by two distinctly different microscopic mechanisms, which are schematically illustrated in the 3D inset in Fig 7a. The first mechanism consists in the detachment of atoms from the highest terrace, their diffusion across the middle terrace and incorporation into the lowest terrace. In the inset, the direction of the overall diffusion flux corresponding to this mechanism is shown by the double solid arrow. Thus, the bridge is formed due to the recombination of the atoms originating from the upper terrace with the vacant atom positions at the lower terrace; in the following, this mechanism is referred to as 'recombination mechanism' (RM). The second, step diffusion mechanism (SDM) consists in a one-dimensional atomic diffusion along each combinatory step, which also leads to blunting of the initially sharp combinatory step corners (near the former intersection point) and, therefore, to bridge broadening. Specifically, SDM consists in the detachment of atoms from the corner of the upper combinatory step, their diffusion along the step and incorporation into the same step at some distance away from the corner. In the inset, the direction of the overall diffusion flux corresponding to SDM is shown by the dashed arrow. Similarly, at the lower terrace, the diffusion of atoms from the periphery towards the corner (not shown) leads to blunting of the lower combinatory step corner and contributes to the bridge widening. This latter process can also be equivalently described as vacancy diffusion away from the corner.

The simulated bridge width kinetics $w(t)$, that well reproduces the experiment at $T = 278$ K and takes into account both RM and SDM, is shown in Fig. 7a with the circle dots. The bridge width evolution $w_{SDM}(t)$ simulated for the same model parameters, but for the pure step diffusion mechanism, is shown in Fig. 7a with the triangular dots. In this latter simulation, the recombination mechanism was artificially suppressed with the help of forbidding atom transfer from the middle to the lowerst terrace through the lower combinatory step by setting an infinitely high Schwöbel barrier [34].

The ratio of SDM contribution $w_{SDM}(t)$ to the total bridge width $w(t)$, that takes into account both mechanisms, is shown in Fig. 7b. It is seen that, at $t \sim 2$ min, the step diffusion mechanism contributes approximately one-third to the total bridge width, and then the SDM contribution monotonically decreases with time down to one-forth at $t = 30$ min. One would expect that, with the increase of bridge width, the effectiveness of the recombination mechanism, which involves atomic diffusion across the bridge, should decrease. However, this expectation is in contradiction with the observed decrease of the ratio w/w_{SDM} with time (Fig. 7b). This fact is in accordance with the notably smaller exponent $\beta = 0.37$ for the SDM kinetics (see Fig. 7a), as compared to the total width kinetics ($\beta = 0.45$). An explanation of this apparent contradiction is that the SDM effectiveness also decreases with time due to the increase of curvature radii of the combinatory step corners. In the limiting case of infinitely large radii corresponding to straight steps, the SDM contribution to the bridge width kinetics is zero. Thus, the decrease of the SDM contribution is faster than the decrease of the RM contribution.

Conclusions

The interaction of vicinal steps and dislocation-induced steps (slip traces), which leads to the anticrossing relief configuration, is shown to be a universal phenomenon observed on the surfaces of a large variety of materials, such as smooth step-terraced vicinal surfaces of simple (Au), compound (Ni_3Al) metals or semiconductors (GaAs). The intersection of a vicinal step with a slip trace results in the formation of a checkered relief configuration consisting of four atomic terraces positioned at three different levels around the crossing point. The uppermost and the lowest terraces are bordered by new angular-shaped combinatory steps. Each combinatory step consists of segments of a former vicinal step and a former slip trace. This configuration with the touching angles of combinatory steps is unstable and, due to diffusion processes, an anticrossing bridge grows. The bridge connects the opposite terraces with the same intermediate level and separates the uppermost and lowest terraces. The kinetics of the anticrossing bridge formation was investigated by UHV-STM on the Au(111) surface and compared to the Monte Carlo simulations. It is shown that the bridge width kinetics is described by a power law dependence $w(t) \sim t^{\beta}$ with the exponent $\beta = 0.45 \pm 0.01$, *i.e.* significantly

lower than the value $\beta = 0.5$ characteristic of a single particle diffusion. Although the comparison of the experimental results with Monte Carlo simulations does not allow one to determine the diffusion activation energy and lateral bond energy separately, we determined the interdependence between these two model parameters, that describes well the anticrossing bridge width kinetics on the Au(111) surface.

We considered two different microscopic mechanisms that may significantly contribute to the anticrossing relief evolution: (1) diffusion of atoms from the uppermost terrace across the bridge and their subsequent incorporation into the lowest terrace (in other words, recombination with vacancies at the lowest terrace), and (2) atomic diffusion along the angular combinatory steps. It turned out that the recombination mechanism dominates over the step diffusion. Moreover, the step diffusion contribution decreases with the increasing bridge width, from approximately one-third at the early stage to one-forth at the mature stage of the observed bridge formation. This unexpected behavior can be explained by the decrease of the step diffusion efficiency induced by the increasing curvature radius of the new combinatory steps. The observed qualitative rearrangement of step-terraced surface morphology due to the interaction between monatomic vicinal steps and slip traces, which leads to the formation of new combinatory steps and anticrossing "bridges", open new opportunities for nanopatterning of surfaces. On the other hand, the anticrossing phenomenon should be taken into account in exploring slip traces for studying elementary mechanisms of plastic relaxation in crystals.

Acknowledgments. This work was partially funded by the French Government program Investissements d'Avenir (LABEX INTERACTIFS, reference ANR-11-LABX-0017-01). Monte Carlo simulations are partially supported by the Ministry of Science and Higher Education of the Russian Federation (Project 0306-2019-0003).

References

[1] A. Pimpinelli, J. Villain, Physics of crystal growth, Cambridge University Press, 1998.

[2] H.C. Jeong, E.D. Williams, Steps on surfaces: experiment and theory, Surf. Sci. Rep. 34 (1999) 171–294.

[3] A.V. Latyshev, A.L. Aseev, A.B. Krasilnikov, S.I. Stenin, Transformations on clean Si(111) stepped surface during sublimation, Surf. Sci. 213 (1989) 157–169.

[4] P. Egberts, R. Gralla, R. Bennewitz, Temporal development of indentation plasticity on the atomic scale revealed by force microscopy, Phys. Rev. B 86 (2012) 035446.

[5] K. Morgenstern, E. Laegsgaard, F. Besenbacher, STM study of step dynamics around a bulk dislocation intersection with a Ag(111) surface, Phys. Rev. B 71 (2005) 155426.

[6] C. Coupeau, J.-C. Girard, J. Rabier, Scanning probe microscopy and dislocations, in: F.R.N. Nabarro, J.P. Hirth (Eds.), Dislocations in Solids 12, Elsevier, 2004, pp. 273–338.

[7] J. Engbæk, J. Schiøtz, Atomic structure of screw dislocations intersecting the Au(111) surface: A combined scanning tunneling microscopy and molecular dynamics study, Phys. Rev. B 74 (2006) 195434.

[8] P. Egberts, R. Bennewitz, Atomic-scale nanoindentation: detection and identification of single glide events in three dimensions by force microscopy, Nanotechnology 22 (2011) 425703.

[9] A. Asenjo, M. Jaafar, E. Carrasco, J.M. Rojo, Dislocation mechanisms in the first stage of plasticity of nanoindented Au(111) surfaces, Phys. Rev. B 73 (2006) 075431.

[10] O.R. de la Fuente, J.A. Zimmerman, M.A. González, J. de la Figuera, J.C. Hamilton, W.W. Pai, J.M. Rojo, Dislocation emission around nanoindentations on a (001) fcc metal surface studied by scanning tunneling microscopy and atomistic simulations, Phys. Rev. Lett. 88 (2002) 036101.

[11] E. Carrasco, O. Rodriguez de la Fuente, M.A. Gonzalez, J.M. Rojo, Dislocation cross slip and formation of terraces around nanoindentations in Au(001), Phys. Rev. B 68 (2003) 180102.

[12] B. Douat, C. Coupeau, J. Bonneville, M. Drouet, L. Vernisse, L. Kubin, Atomic-scale insight into non-crystallographic slip traces in body-centred cubic crystals, Scr. Mater. 162 (2019) 292–295.

[13] S. Yoshida, T. Sekiguchi, K.M. Itoh, Atomically straight steps on vicinal Si(111) surfaces prepared by step-parallel current in the kink-up direction, Appl. Phys. Lett. 87 (2005) 031903.

[14] F. Leroy, D. Karashanova, M. Dufay, J.M. Debierre, T. Frisch, J.J. Metois, P. Muller, Step bunching to step-meandering transition induced by electromigration on Si(111) vicinal surface, Surface Science 603 (2009) 507–512.

[15] A. Pascale, I. Berbezier, A. Ronda, Self-organization of step bunching instability on vicinal substrate, Appl. Phys. Lett. 89 (2006) 104108.

[16] A.M. Andrews, A.E. Romanov, J.S. Speck, M. Bobeth, W. Pompe, Development of cross-hatch morphology during growth of lattice mismatched layers, Appl. Phys. Lett. 77 (2000) 3740–3742.

[17] C. Coupeau, O. Camara, M. Drouet, J. Durinck, J. Bonneville, J. Colin, J. Grilhé, Slip-trace-induced vicinal step destabilization, Phys. Rev. B 93 (2016) 041405.

[18] Y. Nahas, F. Berneau, J. Bonneville, C. Coupeau, M. Drouet, B. Lamongie, M. Marteau, J. Michel, P. Tanguy, C. Tromas, An experimental UHV AFM-STM device for characterizing surface nanostructures under stress/strain at variable temperature, Rev. Sci. Instrum. 84 (2013) 105117.

[19] P. Nozières, Shape and growth of crystals, in: C. Godrèche (Ed.), Solids far from equilibrium, Cambridge University Press, 1992, pp. 1–154.

[20] M.S. Duesbery, The dislocation core and plasticity, in: F.R.N. Nabarro, Dislocations in Solids 8 Basic Problems and Applications, North-Holland, Amsterdam, 1989, pp. 67–174.

[21] I.O. Akhundov, D.M. Kazantsev, V.L. Alperovich, N.S. Rudaya, E.E. Rodyakina, A.V. Latyshev, Formation and interaction of dislocation-induced and vicinal monatomic steps on a GaAs(001) surface under stress relaxation, Scr. Mater. 114 (2016) 125–128.

[22] W.W. Mullins, Theory of thermal grooving, J. Appl. Phys. 28 (1957) 333–339.

[23] H.-C. Jeong, J.D. Weeks, Faceting through the propagation of nucleation, Phys. Rev. Lett. 75 (1995) 4456–4459.

[24] Surface Preparation Laboratory, Penningweg 69-F, 1507 DE Zaandam, The Netherlands

[25] D.V. Brunev, I.G. Neizvestny, N.L. Shwartz, Z.Sh. Yanovitskaya, Influence of Schwöbel barriers and surface diffusion anisotropy on surface relief evolution during epitaxial growth: Simulation, Phys. Low-Dim. Struct. 5 (2001) 173–183.

[26] D.M. Kazantsev, I.O. Akhundov, A.N. Karpov, N.L. Shwartz, V.L. Alperovich, A.S. Terekhov, A.V. Latyshev, Monte Carlo simulation of GaAs(001) surface smoothing in equilibrium conditions, Appl. Surf. Sci. 333 (2015) 141–146.

[27] H. Hoche, J.P. Toennies, R. Vollmer, Combined electron-microscope surface-decoration and helium-atom-scattering study of the layer-by-layer photon-stimulated desorption from NaCl cleavage faces, Phys. Rev. B 50 (1994) 679–691.

[28] K.G. Huang, D. Gibbs, D.M. Zehner, A.R. Sandy, S.G.J. Mochrie, Phase behavior of the Au(111) surface: discommensurations and kinks, Phys. Rev. Lett. 65 (1990) 3313–3316.

[29] V. Repain, J.M. Berroir, S. Rousset, J. Lecoeur, Reconstruction, step edges and self-organization on the Au(111) surface, Appl. Surf. Sci. 162 (2000) 30–36.

[30] J.V. Barth, H. Brune, G. Ertl, R.J. Behm, Scanning tunneling microscopy observations on the reconstructed Au(111) surface - atomic-structure, long-range superstructure, rotational domains, and surface-defects, Phys. Rev. B 42 (1990) 9307–9318.

[31] D. Chauraud, J. Durinck, M. Drouet, L. Vernisse, J. Bonneville, C. Coupeau, Influence of terrace widths on Au(111) reconstruction, Phys. Rev. B 96 (2017) 045410.

[32] H. Göbel, P. von Blanckenhagen, A study of surface diffusion on gold with an atomic force microscope, Surf. Sci. 331–333 (1995) 885–890.

[33] J. Takano, M. Doyama, Y. Kogure, Motion and conversion energies of adatom and adatom clusters on gold (001) surface, Thin Solid Films 424 (2003) 45–49.

[34] M. Benlattar, E. Elkoraychy, K. Sbiaai, M. Mazroui, Y. Boughaleb, Ehrlich-Schwöbel barriers and adsorption of Au, Cu and Ag stepped (100) surfaces, Mod. Phys. Lett. B 31 (2017) 1750037.

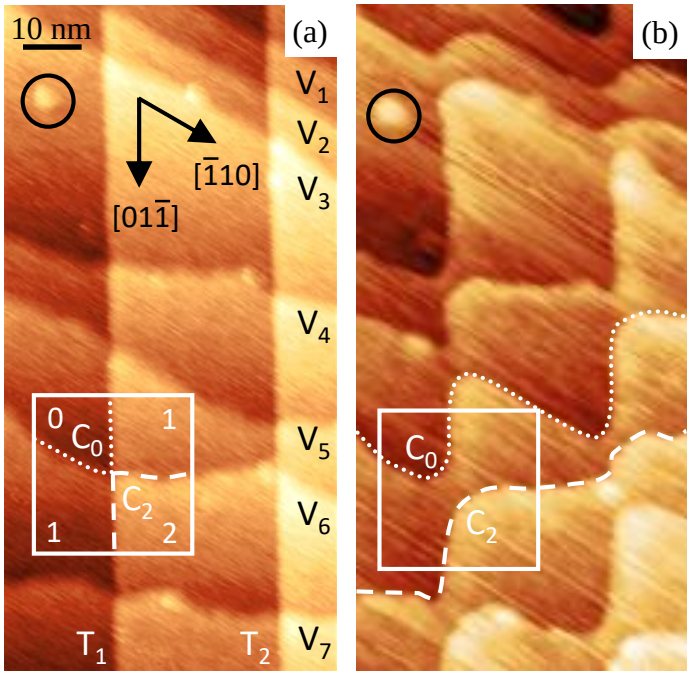

Figure 1: (a) UHV-STM images of Au(111) surface exhibiting intersections of seven curved vicinal steps (labelled from V_1 to V_7) with two straight vertical slip traces (labelled T_1 and T_2) induced by uniaxial compression of the single crystal along the $[\bar{1}10]$ direction at T = 180 K. (b) UHV-STM images of the same area after annealing at T = 300 K for approximately 60 min. The particle marked with the black circle was used as a reference to position the STM images. The white frame highlights the anticrossing phenomenon at the intersection of V_6 and T_1. The numbers 0, 1 and 2 in the white frame indicate the different increasing atomic levels of the associated terraces. The dotted and dashed white lines highlight the combinatory steps labelled C_0 and C_2, respectively.

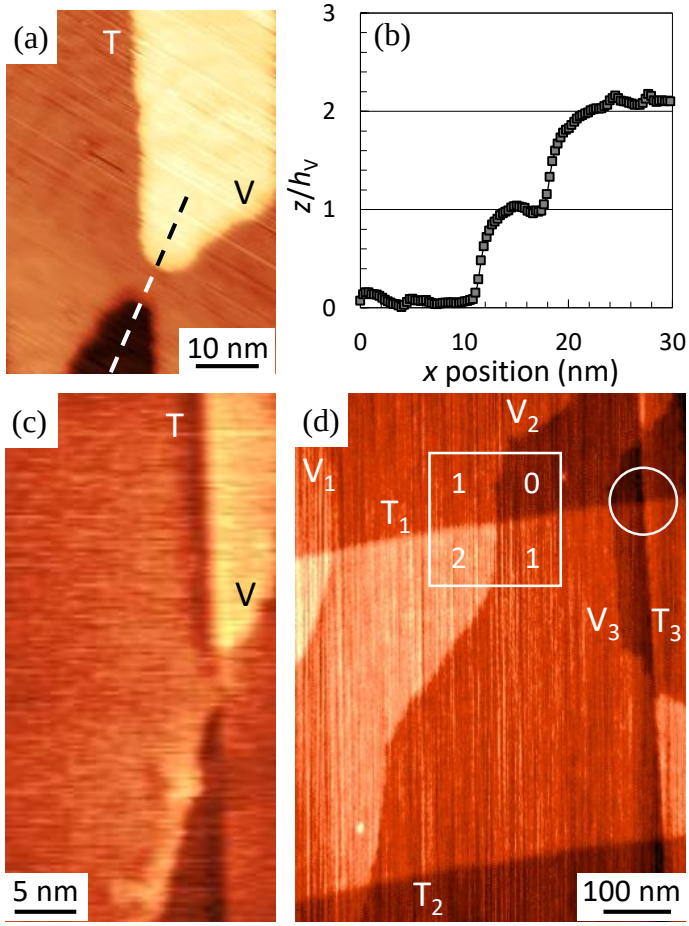

Figure 2: Anticrossing phenomenon occurring on the surfaces of various crystals. (a) STM image of the Au(111) surface around the intersection between a vicinal step V and a slip trace T; (b) *z*-*x* profile across the bridge, along the segment shown in the image (a) with the dashed line, in units of h_V, the vicinal step height; (c) STM image of a similar anticrossing configuration at the $Ni_3Al(111)$ surface; (d) AFM image of the GaAs(001) surface with multiple intersections of vicinal steps (V_1, V_2, V_3) and slip traces (T_1, T_2, T_3). Similar to Fig. 1, the white frame highlights the anticrossing configurations near the intersection between slip trace T_1 and vicinal step V_2. The white circle highlights the intersection between mutually orthogonal slip traces T_1 and T_3. In Figs. 2 (a-d), all vicinal steps and slip traces are of monatomic height, *i.e.* they correspond to the crystal period in the respective crystallographic direction.

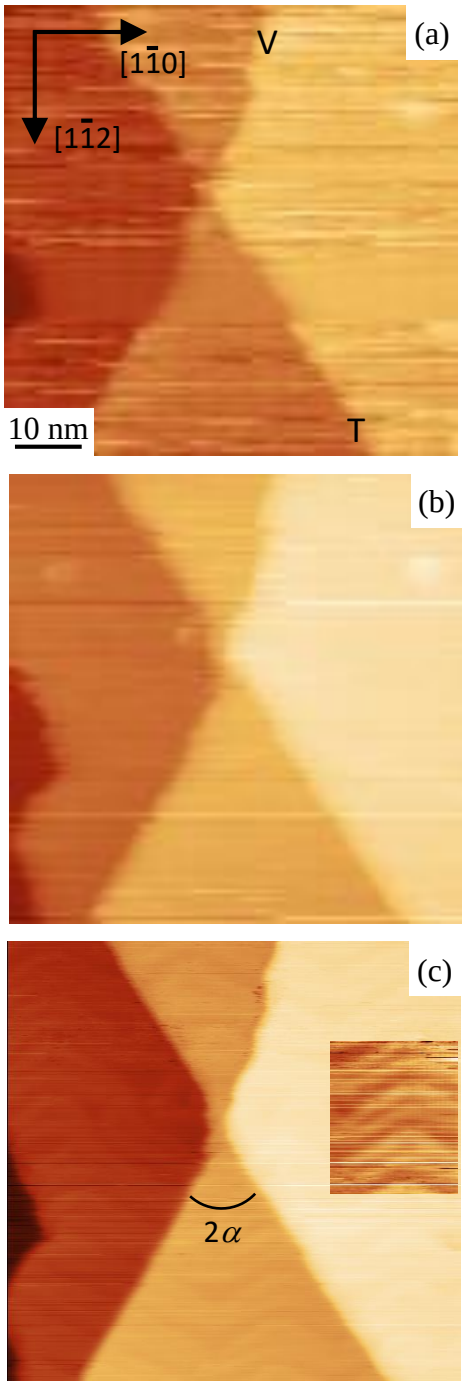

Figure 3: Characteristic kinetic evolution of the Au(111) surface for 2α = 60° during the anticrossing phenomenon (UHV-STM investigations at T = 297 K) at (a) t = 40 s, (b) 370 s and (c) 760 s after the emergence of the slip trace. In the inset, the contrast is enhanced to highlight the well-known herringbone pattern characteristic of the Au(111) atomic reconstruction. V and T correspond to a vicinal step and a slip trace, respectively.

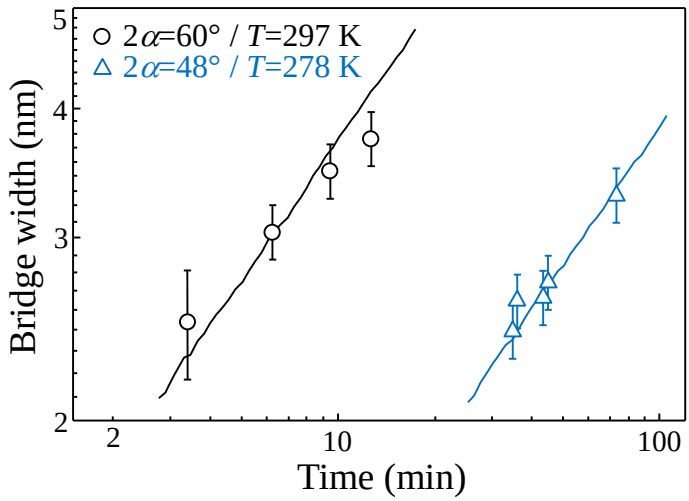

Figure 4: Experimental (dots) and simulated (lines) kinetics of the bridge width on Au(111). The circles correspond to T = 297 K and 2α = 60°, the triangles corresponds to T = 278 K and 2α = 48°. For both temperatures, the solid lines correspond to the Monte-Carlo simulations with E_d = 0.4 eV and E_b = 0.204 eV.

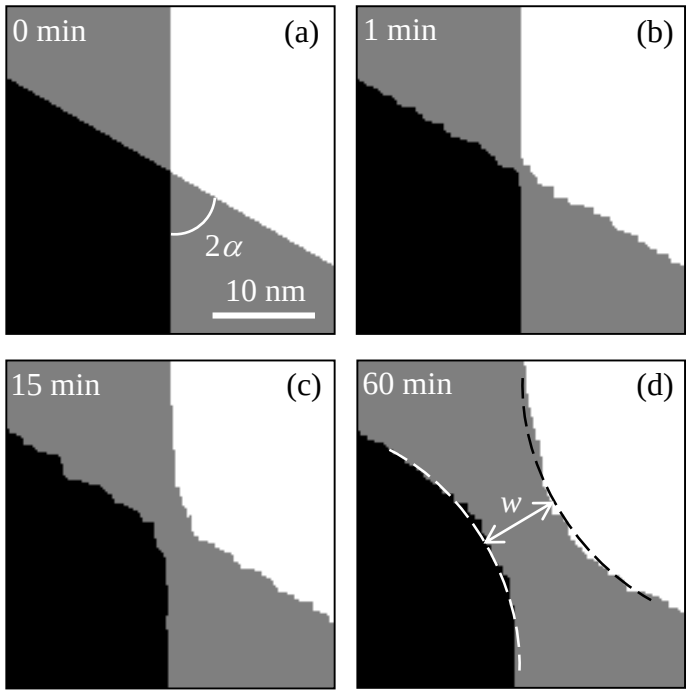

Figure 5: Simulated MC images showing (a) the initial checkered configuration and the bridge growth for various annealing durations: (b) 1 min, (c) 15 min and (d) 60 min. The simulations were carried out at T = 297 K for E_d = 0.4 eV and E_b = 0.204 eV. The circle arcs shown by dashed lines are used to approximate the combinatory steps for bridge width determination (see text).

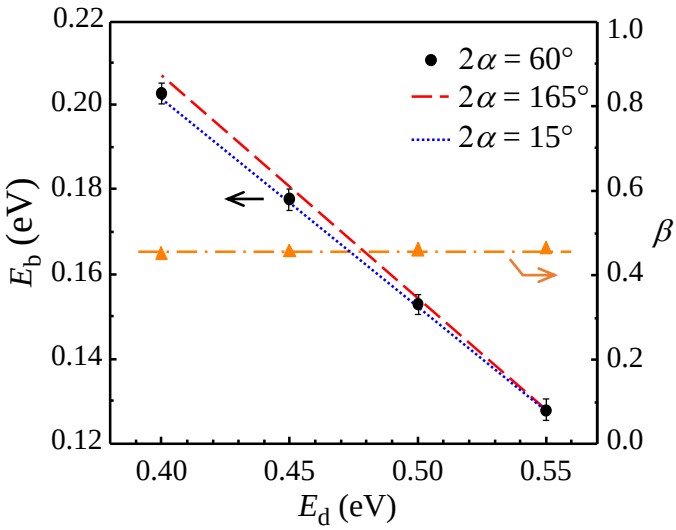

Figure 6: Adatom activation energy E_d *vs*. binding energy E_b for various intersection angles 2α. Experimental data fit is presented with the black circles. Dotted and dashed lines correspond to the MC simulations for $2\alpha = 15°$ and $2\alpha = 165°$, respectively. The power β of the bridge width kinetics for $2\alpha = 60°$ is shown by triangles on the right axis. The dash-dotted horizontal line is drawn as a visual guide for β values.

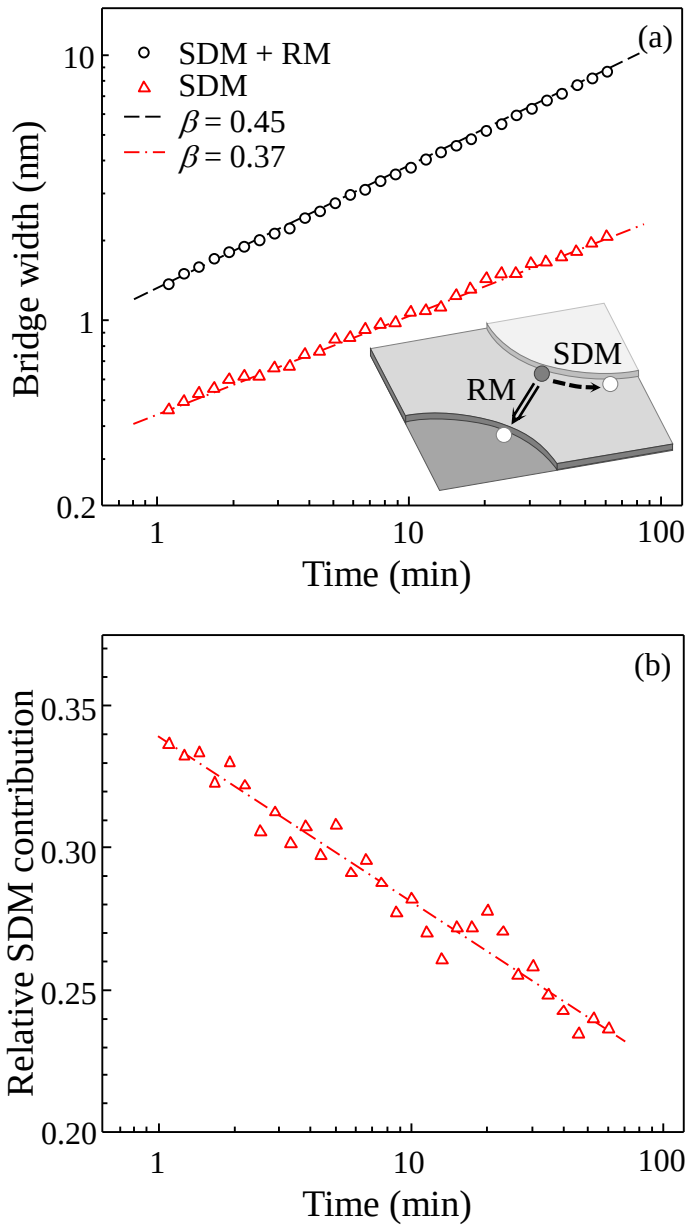

Figure 7: (a) Simulated bridge width kinetics for both recombination (RM) and step diffusion (SDM) mechanisms (circle dots), and for only step diffusion mechanism (triangular dots). Dashed and dash-dotted lines are the power dependence fits with $\beta = 0.45$ and 0.37, respectively. The simulations were performed for $2\alpha = 60°$, $T = 297$ K, $E_d = 0.4$ eV and $E_b = 0.204$ eV. In the inset, RM and SDM mechanisms are schematically illustrated. The directions of the overall diffusion fluxes for RM and SDM are shown by the double solid and dashed arrows, respectively. The initial atom position and the final positions are shown by the dark ball and light balls, respectively. (b) The ratio of the step diffusion contribution to the sum of both contributions.

Combinatory steps (C_0 and C_2) formed due to anticrossing of a vicinal step V and a slip trace T

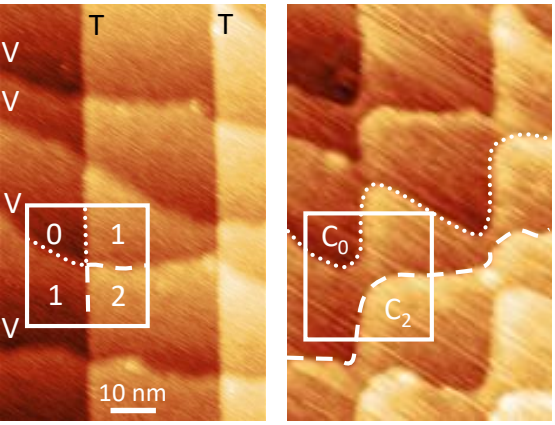

Monte Carlo simulation

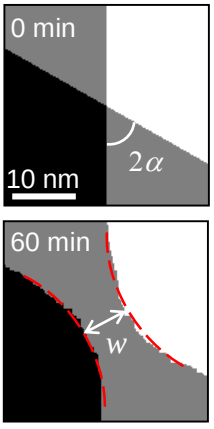

Bridge width kinetics: microscopic mechanisms